

## Mass Ratio Influence on Vortex-Induced Vibration of a Flexible Cylinder using Large Eddy Simulation at $Re=1000$

Avicenna An-Nizhami<sup>1\*</sup>, Nanang Apriandi<sup>1</sup>, Trio Setiawan<sup>1</sup>, Timotius Anggit Kristiawan<sup>1</sup>, Elfrida Rizky Riadini<sup>1</sup>, Atikah Ayu Janitra<sup>1</sup>, Padang Yanuar<sup>1</sup>

<sup>1</sup>Mechanical Engineering Department, Politeknik Negeri Semarang, Jl. Prof. Sudarto, Kota Semarang, 50275

[avicenna@polines.ac.id](mailto:avicenna@polines.ac.id)\*

### Abstract

The study investigates the phenomenon of vortex-induced vibration (VIV) using Large Eddy Simulation (LES) at a Reynolds number of 1000, focusing on transitional flow conditions. LES has proven effective in understanding VIV across Reynolds number regimes, aiding in comprehending flow physics and mechanisms behind VIV. The research aims to contribute data for validating numerical models and informing engineering practices. The study employs the Navier-Stokes equation and the continuity equation to analyze fluid flow, treating it as incompressible due to negligible density changes. The three-dimensional incompressible momentum equation is discretized using the finite volume method within the spatial domain. Resolution of the pressure Poisson equation ensures compliance with free divergence conditions, enhancing computational fluid dynamics simulations' reliability. Validation of the fluid flow solver involves comparing computed drag force coefficients with established benchmarks, showing agreement within small discrepancies. The study delves into vibration behavior induced by cross flow at various reduced velocities ( $U_R$ ), noting distinct patterns ranging from irregularities at low  $U_R$  to quasi-periodic behavior at higher values. Analysis of maximum cylinder displacement ( $y_{max}$ ) across different reduced velocities and mass ratios underscores the complex relationship between system parameters and displacement dynamics. A consistent occurrence of  $y_{max}$  at a specific reduced velocity highlights its significance, while varying mass ratios affect displacement patterns, indicating the importance of understanding these dynamics for optimizing fluid-structure interaction systems.

**Keyword** : Displacement; Large Eddy Simulation; Fluid-Structure Interaction; Vortex-Induced Vibration; Mass Ratio

### Introduction

The investigation of Vortex-Induced Vibration (VIV) within fluid mechanics and engineering has attracted considerable interest due to its significant implications for the design and functionality of diverse structures subjected to fluid dynamics [1]. VIV manifests when a bluff body, like a cylinder submerged in a flowing fluid, undergoes oscillatory forces instigated by the shedding of vortices trailing behind the body. This phenomenon poses significant risks of structural fatigue and potential failure across a spectrum of engineering domains, including offshore platforms, risers, marine cables, bridges, and pipelines.

Vortex shedding within the framework of a cylindrical object submerged in a uniform flow entails a complex fluid dynamic phenomenon where the passage of fluid around the cylinder induces the generation of alternating vortices encircling its form [2]. As the fluid medium interacts with the surface of the cylinder, it engenders oscillations in pressure along its perimeter, leading to the cyclic liberation of vortices downstream. The cyclical shedding of these vortices engenders a characteristic pattern, giving rise to what is commonly referred to as vortex shedding. This intricate process has the potential to elicit vibrations or exert forces that significantly impact the structural integrity and dynamic behaviour of the cylinder. The velocity of the fluid flow, alongside the geometric dimensions of the cylinder and various other pertinent parameters, markedly influences the frequency and distinctive characteristics of the vortex shedding phenomenon. Central to the quantification of the shedding frequency is the Strouhal number, a dimensionless parameter emblematic of the relationship between the shedding frequency, the characteristic length of the cylinder, and the fluid velocity, aptly defined by Equation (1).

$$St = \frac{f_v D}{U_\infty} \quad (1)$$

where  $D$  represents the diameter of the cylinder,  $f_v$  denotes the frequency of vortex shedding, and  $U_\infty$  stands for the free-stream velocity. In the scenario of flow passing around a cylinder, the Strouhal number is additionally influenced by the Reynolds number, defined as Equation (2).

$$Re = \frac{U_\infty D}{\nu} \quad (2)$$

Flow-induced vibration (FIV) can be conceptualized as the oscillatory motion of a cylinder supported by elastic bearings, resulting in transverse and parallel oscillations relative to the flow direction or two degrees of freedom (2-DoF). This modelling approach has been explored by Bishop & Hassan [3], Bearman [4], [5], Sarpkaya [6], [7] and Williamson & Govardhan [8]. Despite the fact that cylinders in reality may oscillate with 2-DoF, FIV models focusing solely on transverse motion are often employed. Studies conducted by Feng [9], Brika & Laneville [10], Khalak & Williamson [11] reveal that the dynamic response of cylinders experiencing FIV is heavily contingent upon the parameters of mass-damping ( $m^* \zeta$ ), where  $m^*$  signifies the ratio of mass displaced by the fluid and  $\zeta$  denotes the damping ratio supporting the cylinder, as defined in Equations (3) and (4).

$$m^* = \frac{4m}{\rho d^2 \pi} \quad (3)$$

$$\zeta = \frac{c}{2\sqrt{km}} \quad (4)$$

Understanding VIV at different Reynolds numbers ( $Re$ ), which characterize the flow regime, is crucial for predicting and mitigating its effects. The Reynolds number represents the ratio of inertial forces to viscous forces in the flow and significantly influences the flow behaviour around a cylinder. At  $Re=1000$ , the flow is typically in the transitional regime, where laminar and turbulent flow characteristics coexist, leading to complex vortex shedding patterns and potentially intriguing dynamics of VIV. To study VIV at  $Re=1000$ , researchers often employ numerical simulations, such as Large Eddy Simulation (LES), which is a computational fluid dynamics (CFD) technique capable of resolving large-scale turbulent structures while modelling the effects of smaller-scale turbulence. LES offers a high-fidelity approach to investigate the complex flow phenomena associated with VIV, capturing the unsteady nature of the flow and its interaction with the cylinder in detail.

Belloli et al. [12] investigated the influence of mass ratio and Reynolds number and the investigation results showcase unexpectedly high oscillation amplitudes in vortex-induced vibrations, highlighting the need for improved data on high mass ratio and high Reynolds number models. Zhao et al. [13] found the vortex-induced vibration of a square cylinder at low Reynolds numbers can be accurately predicted using the finite element method, with the flow approaching angle affecting vibration amplitude and lock-in regime. Bourguet [14] found that flexible cylinders can experience vortex-induced vibrations at subcritical Reynolds numbers, causing unsteady flow and cellular wake patterns, with connections between orbit orientation and flow-structure energy transfer. Wang et al. [15] studied the effect of stiffness nonlinearity. The study found that cubic stiffness nonlinearity affects the vortex-induced vibration of a circular cylinder at low Reynolds numbers, affecting peak amplitude and response envelope. Gu et al. [16] investigated the Reynolds number effects on vortex-induced vibration (VIV) responses. Those are non-negligible and considering them with mass ratio influences can improve engineering applications. Konstantinidis et al. [17] studied vortex-induced in-line vibration at low Reynolds numbers. The study results exhibit resonant amplification within the excitation region, irrespective of the mass ratio value, providing new physical insight. Behara et al. [18] studied VIV of the three staggered circular cylinders, the results exhibit periodic oscillations and nonperiodic vibrations at low Reynolds numbers, with the upstream cylinder showing initial and lower synchronization response modes. Chen et al. [19] researched on the vortex-induced vibrations of tandem cylinders in laminar cross-flow. The research results indicated that the flow can cause wake-induced galloping phenomena, with two distinct vibration patterns observed: vortex-induced vibration and wake-induced galloping. A study

from de Lima [20] found that viscoelastic materials can effectively mitigate vortex-induced vibrations in engineering structures, potentially improving durability and safety.

Previous research has demonstrated the utility of LES in studying VIV across various Reynolds number regimes, providing insights into the flow physics and shedding light on the mechanisms governing VIV. By applying LES to study VIV at  $Re=1000$ , this research aims to contribute to the understanding of VIV in transitional flow conditions and provide valuable data for validating numerical models and informing engineering practices.

## Methodology

### Numerical method

To accurately predict the dynamics of fluid flow, researchers meticulously solve governing equations. These equations, specifically the Navier-Stokes equation (which encompasses the momentum equation and continuity equation), serve as the foundation for fluid dynamics analysis. In this study, the continuity equation—denoted as Equation (5)—approaches fluid flow as incompressible, meaning that density changes are negligible. The three-dimensional incompressible momentum equation, expressed in Equations (6), is implemented in the current study.

To facilitate a comprehensive understanding of fluid behaviour, the researchers employ the finite volume method. This method discretizes the equations within the spatial domain. A critical aspect of this process is determining pressure within the momentum equations. This determination is achieved through the resolution of the pressure Poisson equation. By ensuring the fulfilment of free divergence conditions stipulated by the continuity equation, this crucial step enhances the reliability of computational fluid dynamics simulations.

$$\nabla \cdot \bar{\mathbf{u}} = 0 \quad (5)$$

$$\frac{\partial \bar{\mathbf{u}}_i}{\partial t} + \nabla \cdot (\bar{\mathbf{u}}\bar{\mathbf{u}}) = -\frac{1}{\rho}\nabla p + (\nu + \nu_t)\nabla^2 \mathbf{u} + \mathbf{f} \quad (6)$$

where,  $\bar{\mathbf{u}}_i$  signify the filtered fluid velocity vector,  $p$  represents the filtered fluid pressure field,  $\nu_t$  represents sub grid scale (SGS) eddy kinematic viscosity,

$$\nu_t = (C_s \bar{\Delta})^2 \bar{S} \quad (3)$$

$$\bar{S} = (2\bar{S}_{ij}\bar{S}_{ij})^{\frac{1}{2}} \quad (3)$$

$$\bar{\Delta} = (\Delta x \Delta y \Delta z)^{\frac{1}{3}} \quad (4)$$

where,  $\bar{S}_{ij}$  represents the filtered strain rate tensor,  $C_s$  represents the Smagorinsky constant with  $C_s = 0.18$ .

The structural dynamics of the circular cylinder undergoing a cross flow at Reynolds number equal to 1000 govern by the vibration equation. The vibration equation governs the rate of change of velocity, velocity and displacement of the cylinder.

$$\ddot{y} + \frac{4\pi\zeta}{U_R}\dot{y} + \frac{4\pi^2}{(U_R)^2}y = \frac{2C_y}{\pi m^*} \quad (8)$$

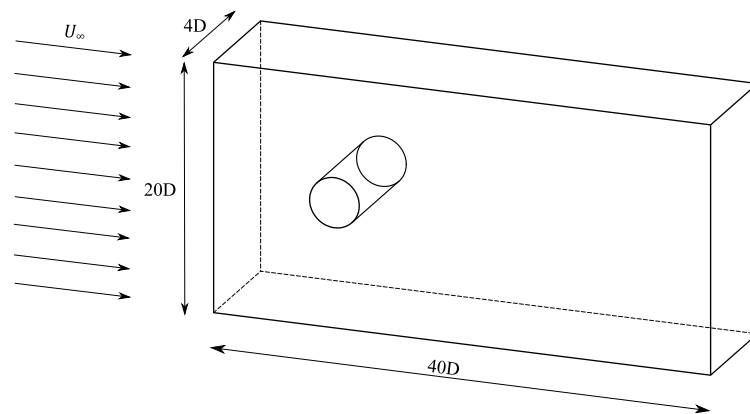
Where  $y$ ,  $\dot{y}$ , and  $\ddot{y}$  signify the cylinder acceleration, velocity, and displacement in transverse direction,  $\zeta$  represents the damping ratio supporting the cylinder,  $U_R$  represents the reduced velocity,  $m^*$  represents the mass ratio of the cylinder to the displaced fluid and  $C_y$  represents the transverse force coefficient. In practical terms, understanding these dynamics is essential for predicting the behavior of structures subjected to fluid forces. Researchers and engineers use such equations to optimize designs, assess stability, and ensure the reliability of various systems.

### Validation of in-house numerical code

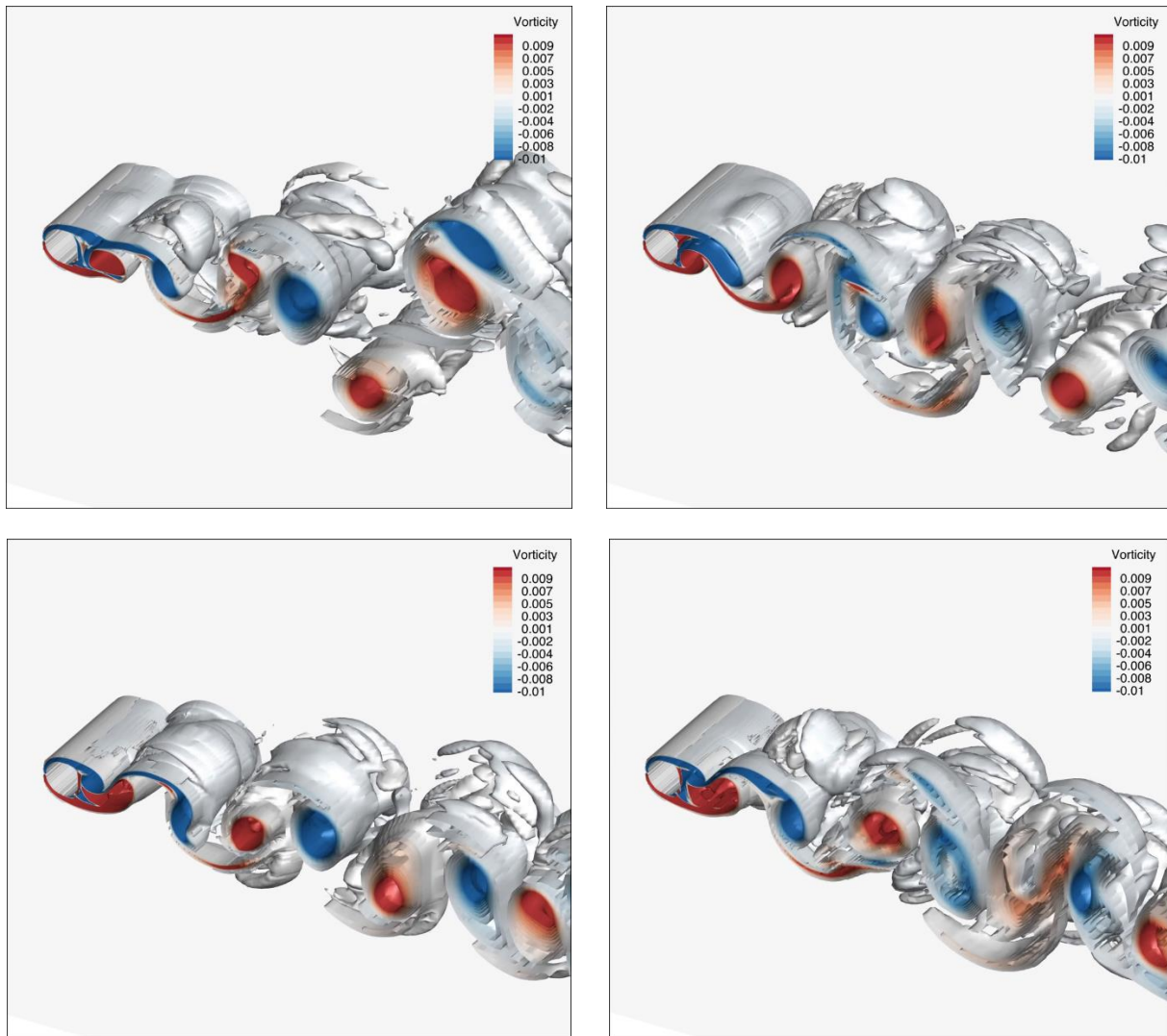
The validation of the fluid flow solver was conducted utilizing a scenario related to the studied case, entailing the flow of a fluid past a stationary cylinder at a Reynolds number of 1000. The parameter under inspection for validation was the drag force coefficient, with its computed value subjected to comparative analysis against established benchmarks, notably those documented by Jordan & Fromm [21] and DynniKova [22]. The outcome of this validation, signifies an agreement between the computed results and the aforementioned benchmark values. The result comparison with the benchmark cases shows minute discrepancies with the percentage of 0.557% and 0.266%. This agreement attests to the efficacy and accuracy of the present numerical methodology in predicting fluid flow dynamics and the forces acting upon the cylinder under consideration at a Reynolds number of 1000.

**Table 1.** The comparison of the average drag force coefficient,  $C_{D,avg}$ , with the benchmark results

Data	$C_{D,avg}$	Discrepancy
Present study	1.246903676	-
Jordan & Fromm [21]	1.24	0.557%
DynniKova [22]	1.2436	0.266%

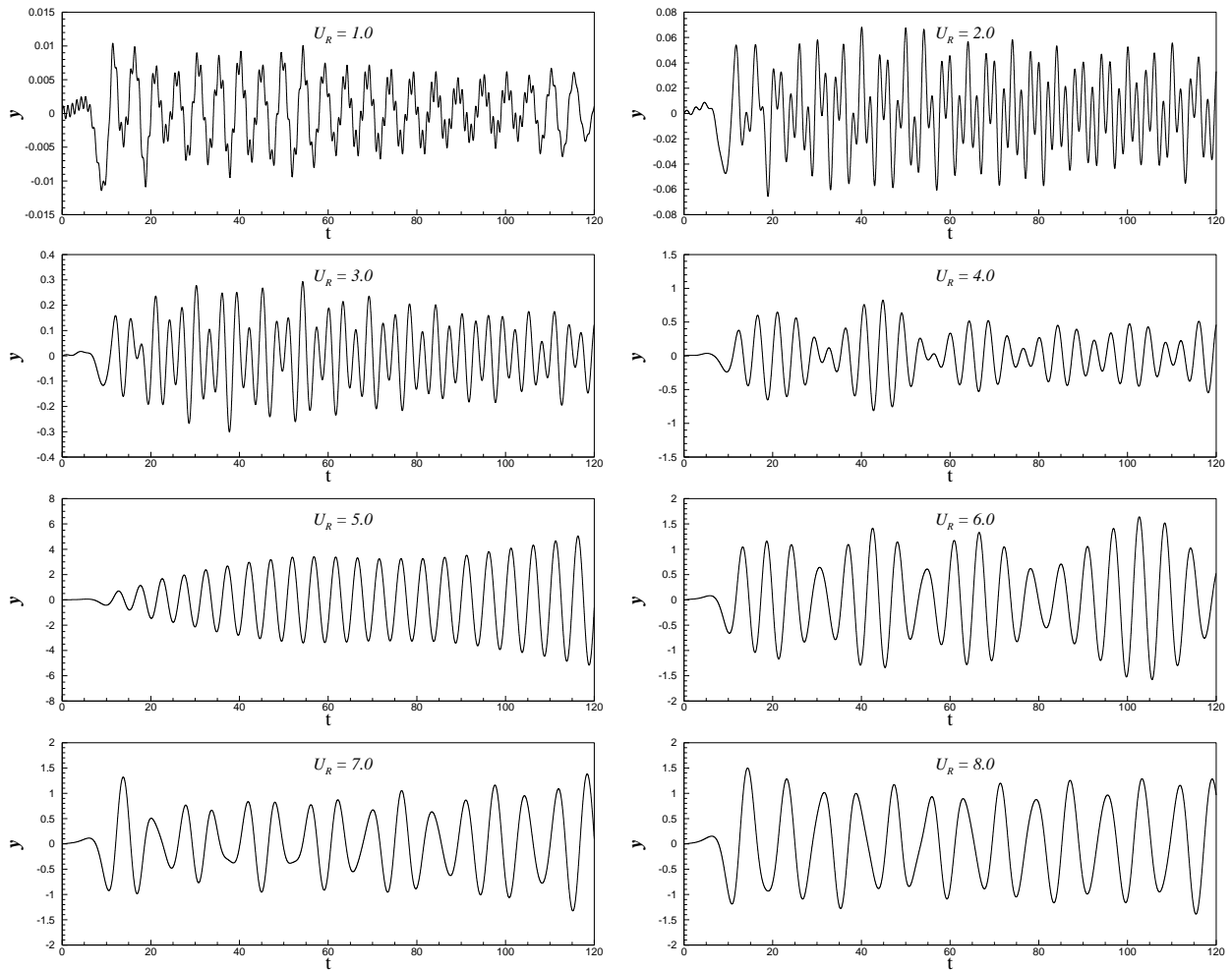


**Figure 1.** Graphical representation of flow past circular cylinder at  $Re=1000$



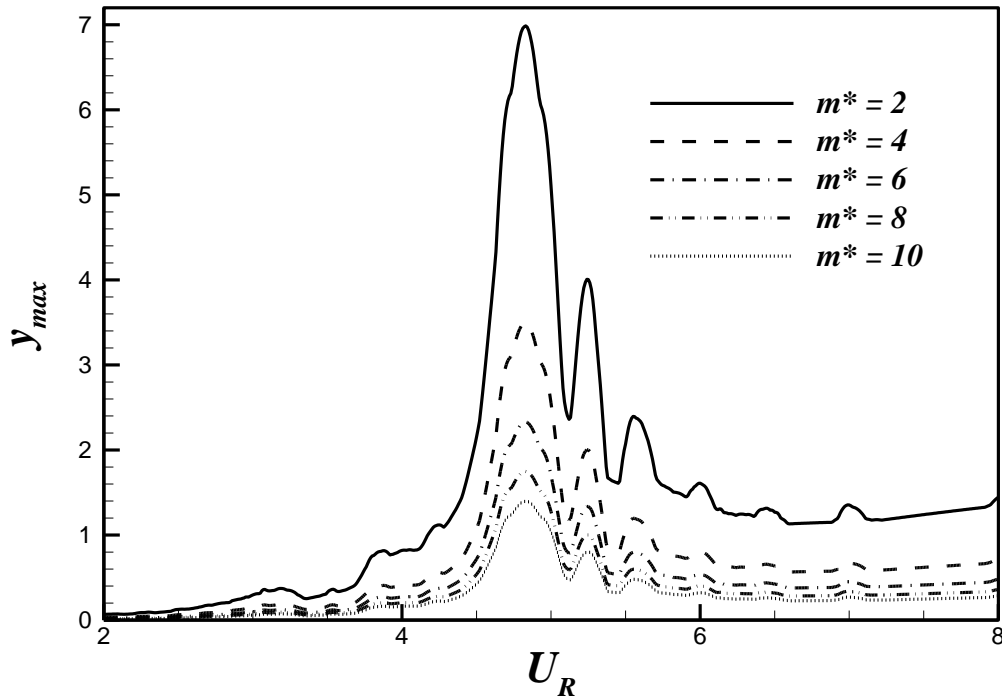
**Figure 2.** Graphical representation of flow past circular cylinder at  $Re=1000$

Figure 2 showcases a cylindrical object submerged in a uniform flow. As fluid flows around the cylinder, it generates alternating vortices encircling the cylinder's form. These vortices result from the shedding of fluid layers as they pass over the cylinder surface. The concept of vorticity, which quantifies the local rotation of fluid elements, is crucial here. Positive vorticity regions (indicated in red) correspond to rotational motion in anticlockwise direction, while negative vorticity regions (blue) represent rotational motion in clockwise direction. These alternating vortices play a pivotal role in the overall fluid behaviour. As the fluid interacts with the cylinder's surface, it experiences oscillations in pressure. These pressure fluctuations occur along the cylinder's perimeter due to the varying flow velocities. When the pressure reaches certain critical points, it triggers the cyclic liberation of vortices downstream.



**Figure 3.** Time history of non-dimensional cylinder displacement within the range of  $1 \leq U_R \leq 8$

Figure 3 illustrates the temporal evolution of cylinder displacement within the range of  $1 \leq U_R \leq 8$ . At  $U_R = 1.0$ , the cylinder displacement exhibits considerable variability and lacks a clear periodic response, characterized by sporadic spikes and disturbances occurring at frequencies surpassing the base frequency. Conversely, for  $U_R = 2.0$ , the cylinder displacement demonstrates a quasi-periodic behavior, featuring drops in amplitude subsequent to reaching peak displacement. Moreover, as the displacement amplitude increases, there is an observable augmentation in the base frequency. Similarly, at  $U_R = 3.0$ , the displacement amplitude displays a tendency to decrease post-peak, albeit to a lesser extent compared to the response observed at  $U_R = 2.0$ . Notably, a beating phenomenon is evident at  $U_R = 4.0$ , manifesting prominently in the initial cycles before gradually diminishing in subsequent cycles. Conversely, at  $U_R = 5.0$ , a notable disparity in the displacement amplitude pattern is observed compared to lower  $U_R$  values, with a slight increase in displacement amplitude over time. Additionally, a beating phenomenon is discernible at  $U_R = 6.0$ , exhibiting a distinct pattern from previous instances, characterized by a gradual increase in the peak amplitude of beating. This trend persists at  $U_R = 7.0$ , where periodic amplitude fluctuations occur, transitioning from higher to smaller amplitudes in successive cycles.



**Figure 3.** The maximum cylinder displacement at all the time to the reduced velocity,  $U_R$ .

The maximum cylinder displacement within the range of  $2 \leq U_R \leq 8$  is illustrated in Figure 3, with varying line types denoting different mass ratio values falling within the range of  $2 \leq m^* \leq 10$ . Notably, the peak value of maximum cylinder displacement, denoted as  $y_{max}$ , consistently occurs at the same  $U_R$  value of 4.83 across all investigated  $m^*$  values. Moreover, the influence of mass ratio on  $y_{max}$  is pronounced, with a discernible trend of diminishing  $y_{max}$  values as  $m^*$  increases, particularly evident at lower  $m^*$  values. This trend underscores the correlation between mass ratio and cylinder displacement dynamics. Despite variations in mass ratio, the overarching pattern of  $y_{max}$  evolution remains consistent, showcasing a characteristic increase with  $U_R$  until it culminates at the peak value corresponding to  $U_R = 4.83$ . Subsequently, as  $U_R$  continues to rise,  $y_{max}$  gradually decreases, indicative of the system's response to increasing fluid flow velocities. Furthermore, beyond the peak, the occurrence of smaller spikes in  $y_{max}$  highlights additional complexities in the dynamic behavior, with the amplitude of these spikes exhibiting a tendency to decrease as  $U_R$  increases. This nuanced understanding of the interdependent relationships between mass ratio, flow velocity, and cylinder displacement is crucial for explaining the underlying mechanisms governing fluid-structure interactions in such systems.

## Conclusion

This study provides a detailed examination of vibration induced by the cross flow at Reynolds number equal to 1000 with the partitioned approach. The observations reveal distinct behaviors at different  $U_R$ , ranging from considerable variability and lack of periodicity at  $U_R = 1.0$  to the manifestation of quasi-periodic behavior at  $U_R = 2.0$ . As reduced velocity increases, the displacement patterns undergo notable changes, including tendencies for post-peak decrease (albeit less pronounced at  $U_R = 3.0$ ), the emergence and diminishment of beating phenomena, and shifts in displacement amplitude patterns. Particularly intriguing is the disparity observed at  $U_R = 5.0$ , where displacement amplitude exhibits a slight increase over time, deviating from the patterns observed at lower reduced velocity. Furthermore, the subsequent analysis of maximum cylinder displacement ( $y_{max}$ ) across reduced velocity ( $2 \leq U_R \leq 8$ ) and varying mass ratios ( $2 \leq m^* \leq 10$ ) underscores the intricate interplay between mass ratio, reduced velocity, and cylinder displacement dynamics. The consistent occurrence of  $y_{max}$  at  $U_R = 4.83$  across different mass ratios highlights the significance of this reduced velocity in dictating peak displacement. Moreover, the influence of mass ratio on  $y_{max}$  reveals a discernible trend of diminishing values with increasing  $m^*$ , further emphasizing the nuanced relationship between system parameters and displacement dynamics. Understanding these dynamics is vital to explain the mechanisms governing fluid-structure interactions and advancing the design and optimization of related systems.

## References

- [1] W. Chen *et al.*, “Investigation of vortex-induced vibrations of rotating cylinders with different surface roughnesses,” *Physics of Fluids*, vol. 36, no. 4, Apr. 2024, doi: 10.1063/5.0197691.
- [2] A. Teimourian and H. Teimourian, “Vortex Shedding Suppression: A Review on Modified Bluff Bodies,” *Eng*, vol. 2, no. 3. Multidisciplinary Digital Publishing Institute (MDPI), pp. 325–339, Sep. 01, 2021. doi: 10.3390/eng2030021.
- [3] Bishop and Hassan, “The lift and drag forces on a circular cylinder oscillating in a flowing fluid,” *Proc R Soc Lond A Math Phys Sci*, vol. 277, no. 1368, pp. 32–50, 1964, [Online]. Available: <https://royalsocietypublishing.org/>
- [4] P. W. Bearman, “Circular cylinder wakes and vortex-induced vibrations,” *J Fluids Struct*, vol. 27, no. 5–6, pp. 648–658, Jul. 2011, doi: 10.1016/j.jfluidstructs.2011.03.021.
- [5] P. W. Bearman, “VORTEX SHEDDING FROM OSCILLATING BLUFF BODIES,” 1984. [Online]. Available: [www.annualreviews.org](http://www.annualreviews.org)
- [6] T. Sarpkaya, “A critical review of the intrinsic nature of vortex-induced vibrations,” *J Fluids Struct*, vol. 19, no. 4, pp. 389–447, 2004, doi: 10.1016/j.jfluidstructs.2004.02.005.
- [7] T. Sarpkaya, “Hydrodynamic Drag, Flow-Induced Oscillations, and Biharmonic Response,” 1995. [Online]. Available: <http://offshoremechanics.asmedigitalcollection.asme.org/>
- [8] C. H. K. Williamson and R. Govardhan, “Vortex-induced vibrations,” *Annu Rev Fluid Mech*, vol. 36, pp. 413–455, 2004, doi: 10.1146/annurev.fluid.36.050802.122128.
- [9] C. C. Feng, “THE MEASUREMENT OF VORTEX INDUCED EFFECTS IN FLOW PAST STATIONARY AND OSCILLATING CIRCULAR AND D-SECTION CYLINDERS,” 1968.
- [10] D. Brika A N and D. A. Laneville, “Vortex-induced vibrations of a long flexible circular cylinder,” 1993.
- [11] A. Khalak and C. H. K. Williamson, “MOTIONS, FORCES AND MODE TRANSITIONS IN VORTEX-INDUCED VIBRATIONS AT LOW MASS-DAMPING,” 1999. [Online]. Available: <http://www.idealibrary.comon>
- [12] M. Belloli, S. Giappino, S. Morganti, S. Muggiasca, and A. Zasso, “Vortex induced vibrations at high Reynolds numbers on circular cylinders,” *Ocean Engineering*, vol. 94, pp. 140–154, Jan. 2015, doi: 10.1016/j.oceaneng.2014.11.017.
- [13] M. Zhao, L. Cheng, and L. Lu, “Vortex induced vibrations of a rotating circular cylinder at low Reynolds number,” *Physics of Fluids*, vol. 26, no. 7, Jul. 2014, doi: 10.1063/1.4886196.
- [14] R. Bourguet, “Vortex-induced vibrations of a flexible cylinder at subcritical Reynolds number,” *J Fluid Mech*, vol. 902, 2020, doi: 10.1017/jfm.2020.676.
- [15] E. Wang, W. Xu, X. Gao, L. Liu, Q. Xiao, and K. Ramesh, “The effect of cubic stiffness nonlinearity on the vortex-induced vibration of a circular cylinder at low Reynolds numbers,” *Ocean Engineering*, vol. 173, pp. 12–27, Feb. 2019, doi: 10.1016/j.oceaneng.2018.12.039.
- [16] J. Gu, A. C. Fernandes, and J. S. Sales, “Alternative insight to understand the Reynolds number effects in vortex-induced vibration,” *Marine Structures*, vol. 69, Jan. 2020, doi: 10.1016/j.marstruc.2019.102686.
- [17] E. Konstantinidis, D. Dorogi, and L. Baranyi, “Resonance in vortex-induced in-line vibration at low Reynolds numbers,” *J Fluid Mech*, 2020, doi: 10.1017/jfm.2020.850.
- [18] S. Behara, B. Ravikanth, and V. Chandra, “Vortex-induced vibrations of three staggered circular cylinders at low Reynolds numbers,” *Physics of Fluids*, vol. 29, no. 8, Aug. 2017, doi: 10.1063/1.4998417.
- [19] W. Chen, C. Ji, J. Williams, D. Xu, L. Yang, and Y. Cui, “Vortex-induced vibrations of three tandem cylinders in laminar cross-flow: Vibration response and galloping mechanism,” *J Fluids Struct*, vol. 78, pp. 215–238, Apr. 2018, doi: 10.1016/j.jfluidstructs.2017.12.017.
- [20] A. M. G. de Lima, B. S. C. da Cunha, A. R. da Silva, and L. F. F. Rodvalho, “Vortex-induced vibration analysis of viscoelastically mounted rigid circular cylinders in cross-flow at a moderate Reynolds number,” *JVC/Journal of Vibration and Control*, vol. 24, no. 13. SAGE Publications Inc., pp. 2688–2700, Jul. 01, 2018. doi: 10.1177/1077546317733656.
- [21] S. K. Jordan and J. E. Fromm, “Oscillatory drag, lift, and torque on a circular cylinder in a uniform flow,” *Physics of Fluids*, vol. 15, no. 3, pp. 371–376, 1972, doi: 10.1063/1.1693918.
- [22] G. Y. Dynnikova, “The lagrangian approach to solving the time-dependent navier-stokes equations,” *Doklady Physics*, vol. 49, no. 11, pp. 648–652, Nov. 2004, doi: 10.1134/1.1831530.